Ceramics-Silikáty 67 (1), 109-119 (2023)
www.ceramics-silikaty.cz doi: 10.13168/cs.2023.0008

PREPARATION OF MAGNESIUM OXIDE AND POTASSIUM MAGNESIUM PHOSPHATE CEMENT FROM LITHIUM-EXTRACTING MAGNESIUM SLAG

WANG JIANLEI*, JIANG XINGHAN*, #WU CHENGYOU*,**

*School of Civil Engineering, Qinghai University, Xining 810016, PR China
**Key Laboratory of Energy-saving Building Materials and Engineering Safety
of Qinghai Province, Xining 810016, PR China

#E-mail: wuchengyou86@163.com

Submitted December 13, 2022; accepted February 17, 2023

Keywords: Magnesium oxide, Lithium-extracting magnesium slag, Potassium magnesium phosphate cement, Impurity ion content, Calcination

MgO was prepared via washing to reduce the impurity of the ion content of the lithium-extracting magnesium slag, a by-product of the Salt Lake and obtained via the membrane separation method, followed by calcination. The MgO was used as a raw material to prepare magnesium potassium phosphate cement (MKPC). Through analyses including X-ray diffraction, scanning electron microscopy, hydration heat release rate, hydration products and porosity, the effects of the impurity of the ion content, and calcination temperature on the physicochemical and MKPC properties of MgO in the lithium-extracting magnesium slag were explored. The results show that the impurity of the ion content and calcination temperature only change the specific surface and crystal morphology of MgO, but not the basic phase composition. The optimal process for the preparation of MKPC from the lithium-extracting magnesium slag included washing to a filtrate the conductivity of 5000 μS·cm^{-1} and calcination at 1200 °C. The MKPC prepared by this combination exhibited the longest setting time, the highest strength in the later stage, and no shrinkage. Regarding its microscopic morphology, the K-struvite structure had the largest size, most regular arrangement, and lowest porosity. This combination was also the most economical and met the requirement of low energy consumption.

INTRODUCTION

Magnesium potassium phosphate cement (MKPC) is a new type of air-hardening cementitious material that typically comprises acid phosphate, dead-burned magnesium oxide, and an appropriate amount of retarder [1]. Compared with other cement materials, MKPC has the advantages of a short hardening time [2], high early strength [3], good cohesion [4-5], and low drying shrinkage [6]. MKPC has been widely used in engineering for rapid repairs [7], reinforcement, refractory material applications, curing of harmful substances [8] and bio-adhesives [9], and national defence engineering construction. However, due to the high energy consumption and cost of dead-burned magnesia powder, the uneven distribution of magnesite resources [10], and rapid acid–base reaction rate with the phosphate solution, the addition of expensive retarders to slow down the process is necessary owing to the rapid solidification rate of the slurry [11]. These shortcomings limit the large-scale application of MKPC. The problem regarding the high raw material cost of MKPC can be solved by using magnesium slag, a by-product of lithium extraction from salt lakes, rather than dead-burned magnesia powder. Furthermore, this will improve the utilisation rate of magnesium resources in salt lakes.

The western salt lakes in Qinghai are rich in brine resources with a low lithium content, a high ratio of magnesium to lithium, and many elements such as boron, potassium, magnesium, and sodium [12]. At present, several successful industrialisation technologies for lithium extraction from brine have been explored, including solvent extraction [13], adsorption [14], precipitation, membrane separation, calcination, and solar pond methods. According to the different driving forces, the membrane separation method can be divided into the nanofiltration membrane (pressure-driven) or electrodialysis (potential-driven) methods and consists of processes for separating, purifying, and concentrating the solute and solvent [15]. When the brine passes through the nanofiltration membrane during the lithium extraction process, monovalent ions such as lithium and sodium pass through the membrane. The nanofiltration membrane separates divalent ions, such as magnesium and calcium, thereby removing the magnesium ions, sulfate radicals, borate radicals, and other impurities to successfully dissolve the magnesium and lithium ions. A large amount of lithium-extracting magnesium slag is produced as a by-product of this process [16].

The main elements in the lithium-extracting magnesium slag extraction process via the membrane separation method are Mg and the coexisting impurity ions Na, K, Cl, and Ca. The coexisting impurity ions will affect the crystallisation characteristics of the MgO during the calcination process. Sivasankari [17] found that K and Na can improve the crystallinity and particle size of the crystals when calcining MgO at 800 °C. Li [18] showed that adding Cl^- in powder preparation can promote the sintering, densification, and grain lengthening of the MgO.

Moreover, the addition of impurity ions is also beneficial to obtain a microstructure with a uniform grain size distribution. NaCl and KCl single salts, or mixed salts, are often used to provide a molten salt environment for liquid-phase combustion synthesis [19]. Eubank [20] studied the effect of different calcination temperatures on the properties of MgO and found that after calcination at 1300 °C, the porosity of MgO decreased and the particle size increased, thereby reducing the solubility of MgO in water. Yang et al. [21] studied the effect of the MgO fineness on MKPC and found that as the specific surface area of the MgO increases, the rate of hydration of the MKPC accelerated, and its setting time shortened. Yang et al. [22] determined that the fineness of the MgO powder and the main particle size of the KH_2PO_4 crystals have a significant effect on the hydration and hardening process of the MKPC slurries; the dissolution and early hydration reaction rates accelerated, and the coagulation time shortened.

In summary, to prepare MgO using lithium-extracting magnesium slag, the impurity ions of the magnesium slag and calcination temperature will affect not only the properties of the generated MgO, but also the properties of the magnesium cement. This requires further detailed research and analysis.

In this study, the MgO and MKPC were prepared from lithium-extracting magnesium slag, a by-product of lithium extraction via the membrane separation method. The results of the compressive strength, setting time, porosity, and hydration were used to ascertain the effects of the impurity ion content in the magnesium slag and calcination temperature on the MKPC. Determine the best MgO preparation process according to the performance and economic benefits of the MKPC. The study provides a theoretical basis for the production of a low-cost, retarder-free MKPC from the by-products of lithium extraction from salt lake brine and promotes the circular production and comprehensive utilisation of salt lake resources, which can alleviate the ecological pressure of Salt Lake to a certain extent, it provides a reference for the preparation of MgO and MKPC in Northwest China.

EXPERIMENTAL

Raw materials

(1) The lithium-extracting magnesium slag was purchased from Qinghai Salt Lake Industry Co., Ltd. The by-products of the lithium extraction, obtained by extracting the lithium resources of the Chaerhan Salt Lake via the membrane separation method, and the composition of the element ions are listed in Table 1. The X-ray diffraction (XRD) pattern in Figure 1 shows that the main phase compositions were $Mg(OH)_2$, NaCl, $MgCl_2$, and KCl and that there are more chloride salt impurities.

Table 1. Elemental ion composition of the lithium-extracting magnesium slag.

Ionic composition	Mg^{2+}	Na^+	Cl^-	Ca^{2+}	K^+
Mass fraction (%)	31.01	1.06	9.50	0.36	0.14

(2) The potassium dihydrogen phosphate KH_2PO_4, the analytical reagent, was purchased from the Hongyan Reagent Factory, Hedong District, Tianjin.

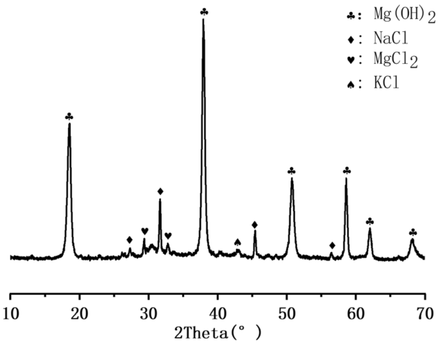

Figure 1. XRD pattern of initial lithium-extracting magnesium slag.

Preparation and characterisation of MgO

First, the content of the various impurities in the lithium-extracting magnesium slag was reduced by washing filtration. Then, the conductivity value of the filtrate obtained during the washing process was used as the evaluation standard for the impurity ion content in the lithium–magnesium extraction slag. Three groups of lithium-extracting magnesium slags with different impurity ion contents were obtained, designated G100, G50, and G20, representing 10000, 5000, and 2500 $\mu S \cdot cm^{-1}$, respectively. After cleaning, the lithium-extracting magnesium slags with the different impurity ion contents were dried and ground, and then subjected to X-ray fluorescence spectrometry (XRF).

Table 2 lists the XRF analysis results. The conductivity and Cl^- content decreased continuously.

Table 2. XRF analysis results of the lithium-extracting magnesium slag after cleaning.

Sample	MgO	CaO	Cl^-	LOI
G25	96.2	3.30	0.182	0.318
G50	96.1	3.15	0.364	0.386
G100	95.7	2.83	0.998	0.472

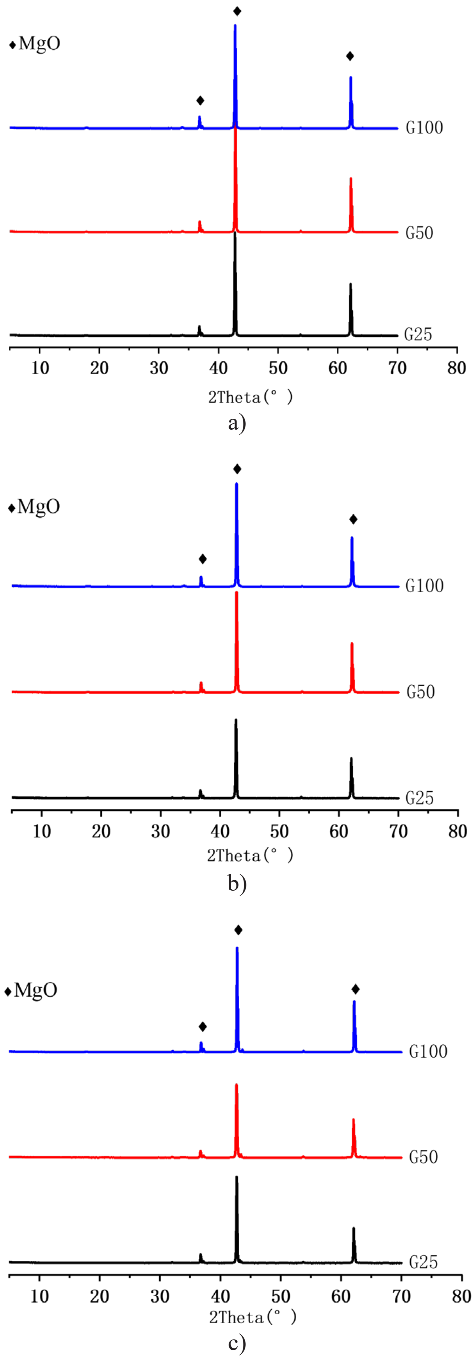

a)

b)

c)

Figure 2. XRD patterns of the MgO prepared by the different processes: (a) T11, (b) T12, and (c) T13.

Table 3. Quantitative analysis results of the MgO prepared by the different processes.

Calcination temperature	Impurity ion content	MgO (%)	CaO (%)	NaCl (%)
T11	G100	99.0	0.8	0.2
	G50	98.6	1.3	0.1
	G25	98.7	1.3	0.0
T12	G100	98.8	1.0	0.2
	G50	98.5	1.4	0.1
	G25	98.5	1.5	0.0
T13	G100	98.3	1.5	0.2
	G50	98.2	1.7	0.1
	G25	98.3	1.7	0.0

The dried lithium-extracting magnesium slag was loaded into a corundum crucible and placed in a muffle furnace at T11, T12, and T13, representing the three calcination temperatures of 1100, 1200, and 1300 °C. Afterwards, the MgO for the experiment was obtained. Since the sintering temperature is higher than the decomposition temperature, all the $Mg(OH)_2$ is transformed into MgO. At 1000 °C, the compounds such as NaCl and KCl coexisting in the magnesium slag have melted and transformed into a liquid phase. Figure 2 shows the XRD patterns of the MgO obtained from the lithium-extracting magnesium slag after these various processes. The spectrum shows that the main diffraction peak is MgO. The impurity ion content and calcination temperature of the magnesium slag will not change the basic phase composition of the generated MgO; however, the limited performance and obscure spurious peaks indicate a need for the quantitative analysis of the XRD of the lithium-extracting magnesium slag MgO. Table 3 lists the results of the quantitative analysis of the MgO prepared via the various processes using the Jade 6.5 software. The results listed in Table 3 indicate that, under the same calcination temperature, the CaO content in the MgO of G100 was significantly smaller than that of G50 and G25, whereas the CaO content in the MgO of G50 and G25 was similar. In addition, the NaCl content in the prepared MgO decreased sequentially with the conductivity. Under the same impurity ion content, an increase in the calcination temperature resulted in a decrease in the purity of the MgO, a sequential increase in the CaO content, and an unaffected NaCl content.

Table 4 lists the specific Brunauer-Emmett-Teller (BET) method surface areas of the MgO prepared with the different impurity ion contents and different calcination temperatures. The data show that, at the same calcination temperature, the specific surface area of the MgO in G100 was smaller than that of G50 and G25, whereas the difference between the specific surface areas of the MgO in G50 and G25 was small. When the impurity ion contents were the same, the specific surface area of the MgO decreased significantly with an increase in the calcination temperature. This

Table 4. Specific surface area of the MgO.

Calcination temperature	Impurity ion content	BET surface area ($m^2 \cdot g^{-1}$)
T11	G100	1.3575
	G50	1.4533
	G25	1.4525
T12	G100	0.7450
	G50	0.8835
	G25	0.8468
T13	G100	0.4038
	G50	0.5023
	G25	0.5362

indicated that the effect of the calcination temperature on the specific surface area of the MgO was significantly greater than that of the impurity ion content, which can more effectively reduce the specific surface area of the MgO, thereby increasing the setting time of the MKPC. Figure 3 shows the microscopic images of the MgO prepared via the various processes. From Figure 3a, b, when the calcination temperature is the same, there is no obvious difference in the microstructure of the MgO for the different impurity ion contents. From Figure 3b, c,d, as the calcination temperature increased, the MgO grains were sintered, and the grains began to bond and swallow each other for crystal reorganisation. The shapes were more regular spherical crystals. The grains gradually tended to become edged polyhedrons, the size increased, the arrangement became loose, the crystal structure became more compact and perfect, and the specific surface area decreased.

Specimen preparation

First, the pre-ground KH_2PO_4 and MgO were placed into a mortar and uniformly mixed according to a ratio of magnesium to phosphorus $m(MgO)/m(KH_2PO_4) = 4.5$. Then, an appropriate amount of deionised water was added according to a water-to-cement ratio of 0.2 and stirred evenly to form an MKPC slurry. The slurry was mixed for 2 minutes until the bubbles in the slurry had disappeared, poured into a steel mould with dimensions of 20 mm × 20 mm × 20 mm, and cured at 20 ± 2 °C with a relative humidity of 50 ± 5 %. After curing for 3 h, the slurry was demoulded and the cube compressive strength of the MKPC specimens was immediately tested. After demoulding, the remaining specimens were naturally cured in the air until they reached the required age. The samples are expressed as “GT”, where “G” represents the conductivity of the magnesium slag filtrate,

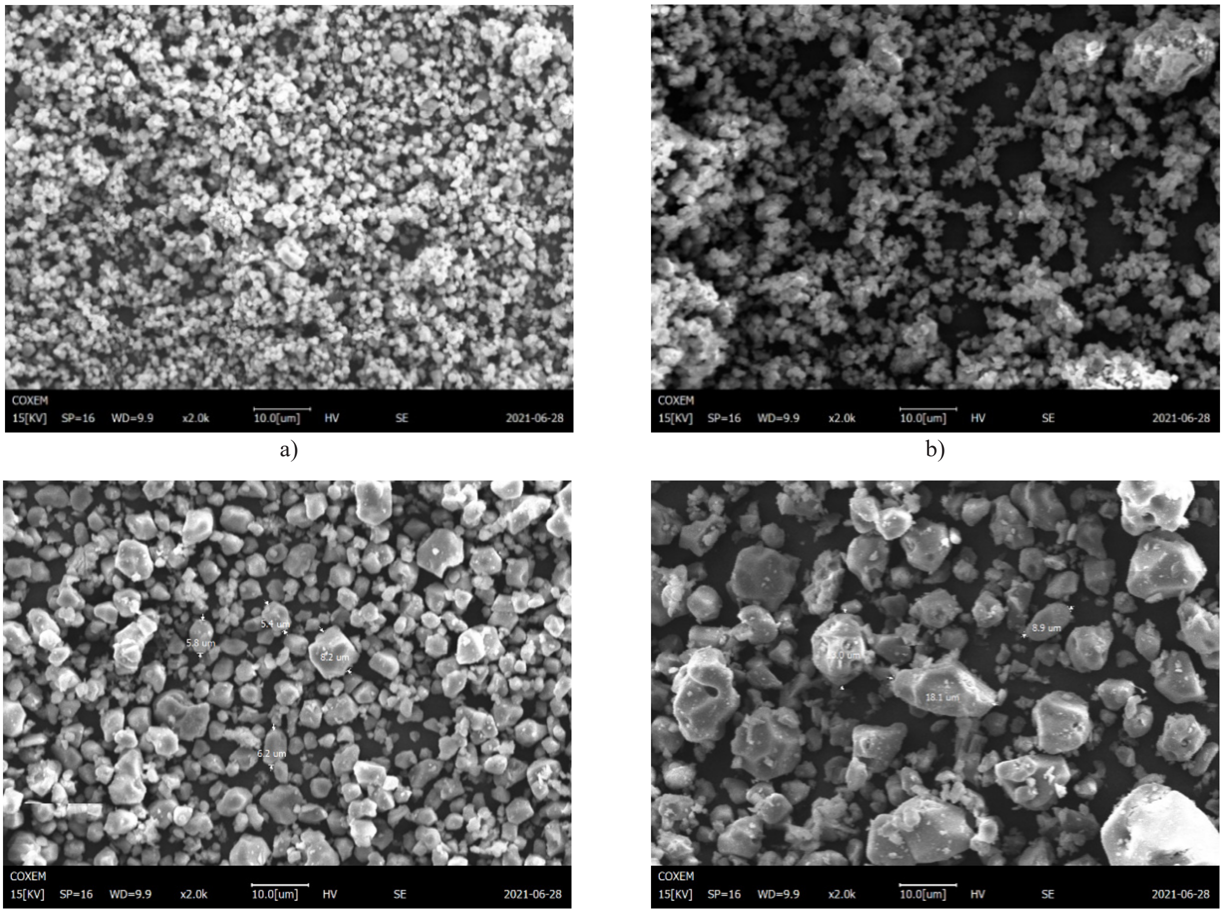

a)

b)

c)

d)

Figure 3. Microscopic images of the MgO (a) G25T11, (b) G100T11, (c) G50T11 and (d) G50T12.

indicating that the impurity ion content differs; and "T" represents the calcination temperature of the lithium-extracting magnesium slag. For example, G50T12 represents an MKPC test sample with an impurity ion content of the lithium-magnesium slag washed to a filtrate conductivity of 5000 µS·cm^{-1} and a calcination temperature of 1200 °C.

RESULTS AND DISCUSSION

Setting time of the MKPC

Figure 4 shows the effects of the different impurity ion contents and calcination temperatures on the setting time of the MKPC. Due to the short interval between the initial and final setting times of the MKPC, only the initial setting time was determined in this experiment and used as a criterion. Figure 4a shows that, for the different impurity ion contents in the magnesium slag, the setting time of the MKPC prepared using G50 was higher than that of the other two groups when calcined at the same temperature, indicating that the content of the impurities, such as NaCl, in G50 was higher than that of the other two groups, which is conducive to prolonging the setting time of the MKPC. Figure 4b shows the setting time of the different magnesium slag impurity ion contents at different calcination temperatures; the setting time of the MKPC increased substantially with an increase in the calcination temperature from T11 to T12. However, when the calcination temperature increased from T12 to T13, the setting time did not change substantially. Therefore, an increase in the calcination temperature from T11 to T12 causes the grain size of the MgO to become larger, the specific surface area to decrease, the degree of MgO crystallisation to increase, and the corresponding activity to reduce, thereby reducing the reaction rate, which can effectively extend the setting time of the MKPC. When the calcination temperature was increased from T12 to T13, the specific surface area and activity of the MgO changed marginally; thus, the setting time did not change significantly.

Compressive strength of the MKPC

Figure 5 shows the cubic compressive strength of the MKPC specimens. Figure 5 shows that under the same calcination conditions, the later strength of the MKPC specimen prepared using G50 was higher than that of G25 and G100. For example, when calcined at T11, the compressive strengths of G50T11, G25T11, and G100T11 at a curing age of 28 d were 77.6, 71.2, and 69.5 MPa, respectively; thus, G50T11 was 9.0 % and 11.7 % stronger than the G25T11 and G100T11 specimens, respectively. This can be explained by the impurity ion content of the lithium-extracting magnesium slag having an influence on the cubic compressive strength of the MKPC specimens, and an impurity ion content that is too high or too low is not conducive to improving the later strength of the MKPC. G50 was the most conducive to the late strength development of the MKPC.

Figure 5 shows that, under the same impurity ion content, the compressive strength of the MKPC specimens prepared by firing the lithium-extracting magnesium slag at T11 for 3 h is initially higher than that of T12 and T13; the compressive strength was in the order of T13 > T12 > T11 at 28 d. The compressive strengths of the G25T11, G25T12, and G25T13 specimens at 3 h were 58.0, 40.1, and 27.8 MPa, respectively; thus, G25T11 was 30.9 % and 52.1 % stronger than the G25T12 and G25T13 specimens, respectively. Furthermore, the compressive strengths of the G25T13, G25T12, and G25T11 specimens at 28 d were 79.8, 74.9, and 71.2 MPa, respectively; thus, G25T13 was 6.5 % and 12.1 % stronger than the G25T12 and G25T13 specimens, respectively. This phenomenon indicates that the lower the calcination temperature, the higher the early strength of the MKPC, although it is not conducive to the later strength development; conversely, the higher the calcination temperature, the higher the later strength of the MKPC. This is mainly because the MgO activity obtained by calcining the lithium-extracting magnesium slag at T11 is higher and the specific surface area is larger; thus, as the hydration reaction rate

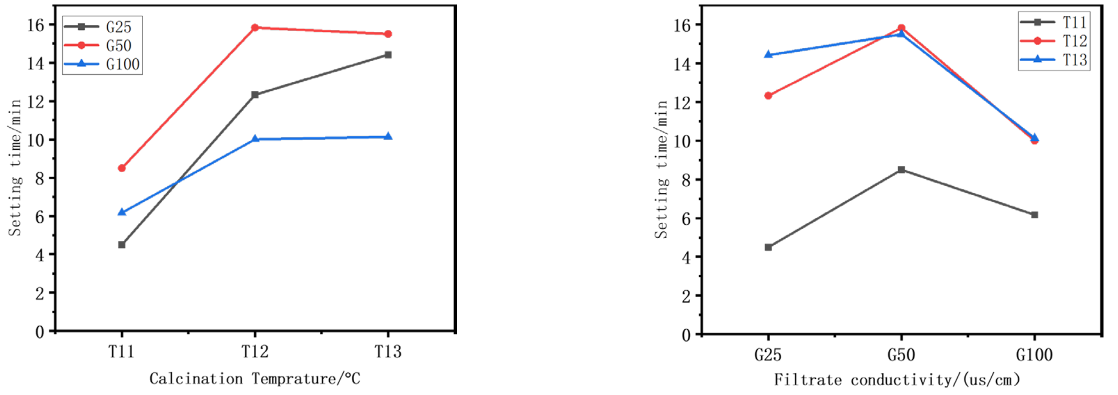

a) b)

Figure 4. Effect of (a) the impurity ion content and (b) calcination temperature (b) on the setting time of the MKPC.

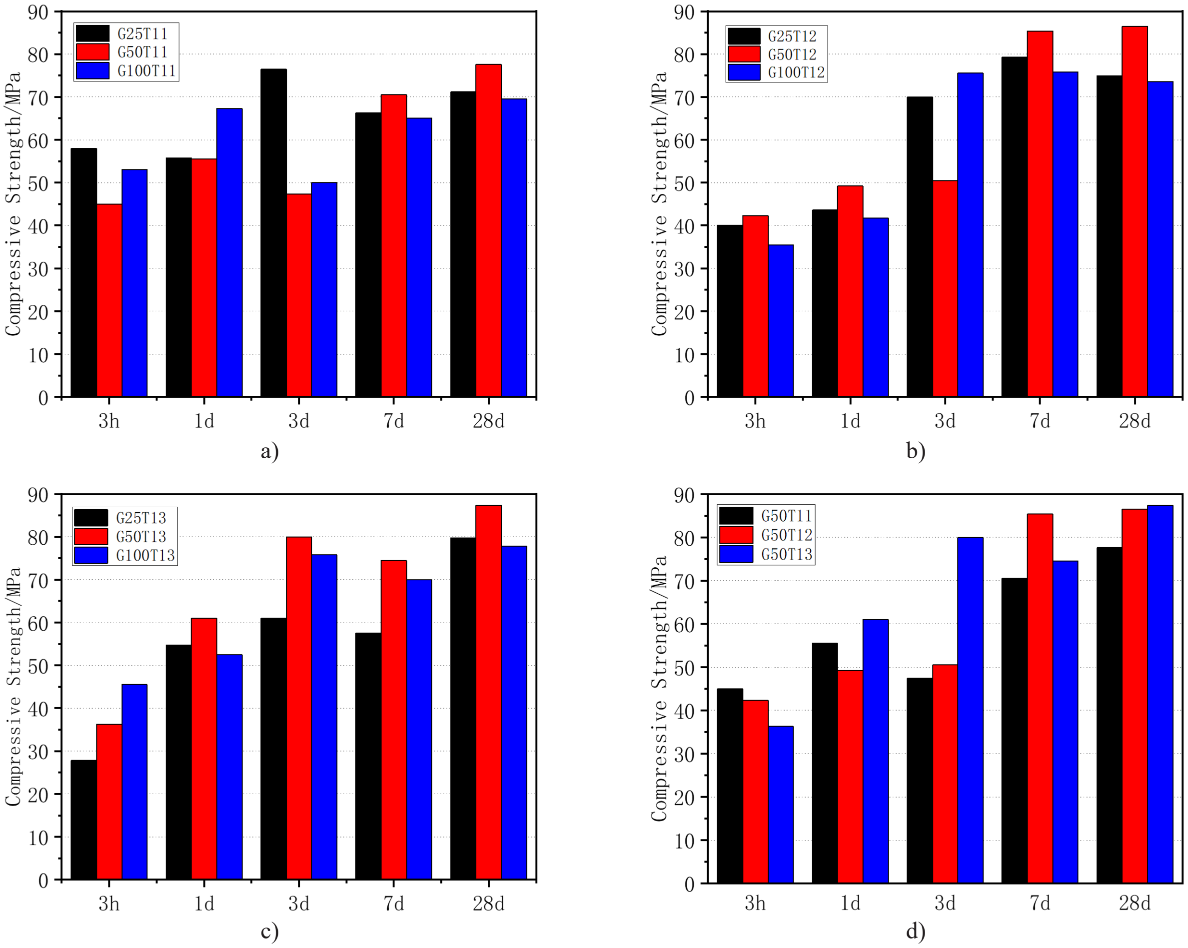

a) b) c) d)

Figure 5. Cubic compressive strength of the MKPC specimens: (a) T11, (b) T12, (c) T13, (d) G50.

of the MKPC is faster, the reaction is intense, the setting time is short, and the early strength will be higher. Along with the hydration reaction, the temperature of the MKPC slurry rises rapidly, resulting in a large temperature stress that renders the MKPC structure susceptible to temperature cracks, which is not conducive to the development of late strength. Conversely, the behaviour of the MgO obtained via calcination at the higher temperatures is the opposite, with a lower activity, smaller specific surface area, slower hydration reaction than at T11, and late steady strength growth.

Exothermic hydration of the MKPC

Figure 6 shows the hydration temperature tracking curve of the MKPC. The exothermic hydration of the MKPC in the first 3 h can be divided into four stages. During the first stage, KH_2PO_4 is rapidly dissolved in water to obtain K^+ and H_2PO^{4-}, while H_2PO^{4-} is ionised to obtain H^+ and HPO_4^{2-}, the MgO started to hydrate rapidly and quickly released a large amount of heat; the duration of which was approximately 2 to 6 min. At the end of the first stage, the MKPC hydration and heat release resulted in the first exothermic peak. In the second stage, the exothermic rate of the MKPC decreased sharply. The duration of this stage was approximately 20 to 25 min. At the end of this stage, the exothermic curve reached the first valley. In the third stage, generates $MgKPO_4·6H_2O$, the MKPC released heat to the exterior at a slower exothermic rate than that of the first stage, and the total heat release was smaller. At the end of the third stage, the exothermic curve reached the second exothermic peak. In the fourth stage, the exothermic rate of the MKPC decreased slowly, and the hydration reaction tended to be stable. The ionisation equation is as follow:

$$KH_2PO_4 \rightarrow K^+ + 2H^+ + PO_4^{3-} \tag{1}$$

$$MgO + H_2O \rightarrow MgOH^+ + OH^-$$
$$Mg^{2+} + 6H_2O \rightarrow Mg(H_2O)_6^{2+} \tag{2}$$

$$Mg(H_2O)_6^{2+} + PO_4^{3-} + K^+ \rightarrow MgKPO_4 \cdot 6H_2O \tag{3}$$

Figure 6a, b, c shows that irrespective of the calcination temperature adopted, the time of the appearance of the first exothermic peak in the hydration curve of the MKPC for each impurity ion content did not

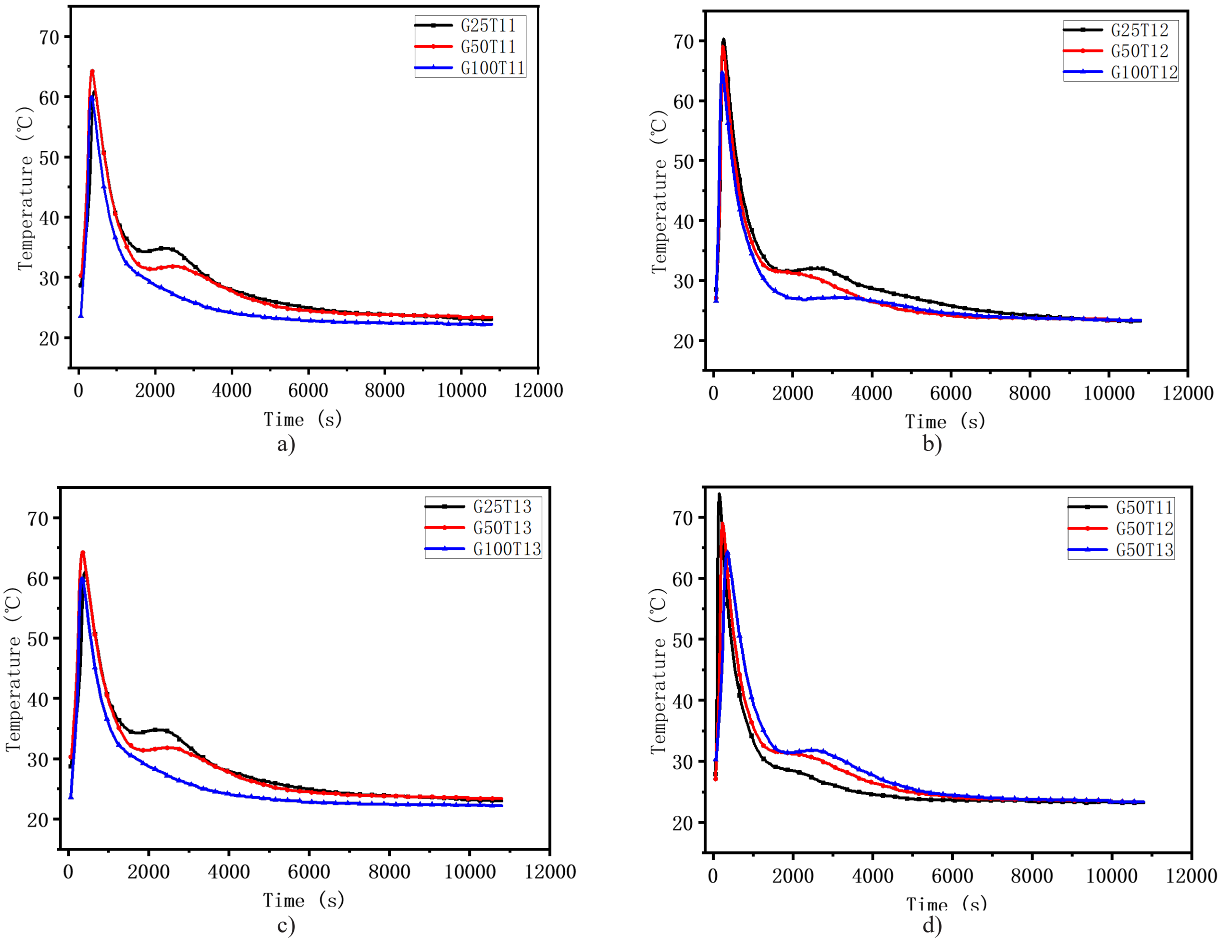

a) b) c) d)

Figure 6. Hydration temperature tracking curve of the MKPC: (a) T11, (b) T12, (c) T13, (d) G50.

differ significantly. Figure 6d shows that an increase in the calcination temperature corresponds to a delay in the time of the first exothermic peak of the MKPC hydration. This increase can reduce the maximum temperature during the hydration process of the MKPC. For example, as shown in Figure 6d, the hydration exothermic curves of G50T11, G50T12, and G50T13 had their first exothermic peaks appearing at 2.35, 3.8, and 5.63 min, respectively. Compared to G50T11, the time of the first exothermic peaks for G50T12 and G50T13 was delayed by 61.7 % and 139.6 %, respectively. The temperature magnitude of the first exothermic peak of the MKPC also decreased from 73.9 for G50T11 to 69.1 and 64.3 °C, a decrease of 6.5 % and 13.0 % for G50T12 and G50T13, respectively. Therefore, an increase in the calcination temperature can reduce the exothermic rate and heat release during the hydration process of the MKPC, which is beneficial in delaying the setting time of the MKPC. Figure 6 shows that the temperature of the calcined lithium-extracting magnesium slag had a great influence on the hydration heat of the MKPC, whereas the influence of the impurity ion content was small. This phenomenon indicates that increasing the calcination temperature can effectively delay the exothermic reaction in the first and third stages of the MKPC temperature tracking curve and delay the dissolution of the MgO in an acidic environment and the formation of the hydration product $MgKPO_4 \cdot 6H_2O$.

Hydration products of the MKPC

Figure 7 plots the XRD patterns of each MKPC group after 28 d of curing. Figure 7 demonstrates that the strong characteristic peaks of MgO can be observed with no significant difference in the peak positions in each group. The MgO content in the whole reaction system was too high with a significant amount of unreacted MgO in the cement sample and a significant amount of excess MgO crystals in the MKPC specimen in the later stage of hydration, which also played a role in the final structure. In the MKPC system, the hydration products are relatively simple. The characteristic peaks representing the MKPC can also be found in the XRD, and they were observed to undergo no significant changes for the different impurity ion contents and calcination temperatures. From the XRD pattern, the diffraction peaks of the MgO and MKP could be observed; however, there were a few phase peaks that were not obvious; thus, the XRD of the MKPC was quantitatively analysed.

Table 5. Quantitative analysis results of the MKPC after 28 d.

Sample	MgO (%)	$MgKPO_4{\cdot}6H_2O$ (%)	$CaCO_3$ (%)
G100T11	57.6	39.2	3.2
G100T12	57.0	40.0	3.0
G100T13	55.3	41.8	2.9
G500T11	56.7	40.7	2.6
G50T12	55.2	42.5	2.3
G50T13	54.8	43.0	2.2
G25T11	54.5	44.2	1.3
G25T12	53.2	45.8	1.0
G25T13	50.2	49.0	0.8

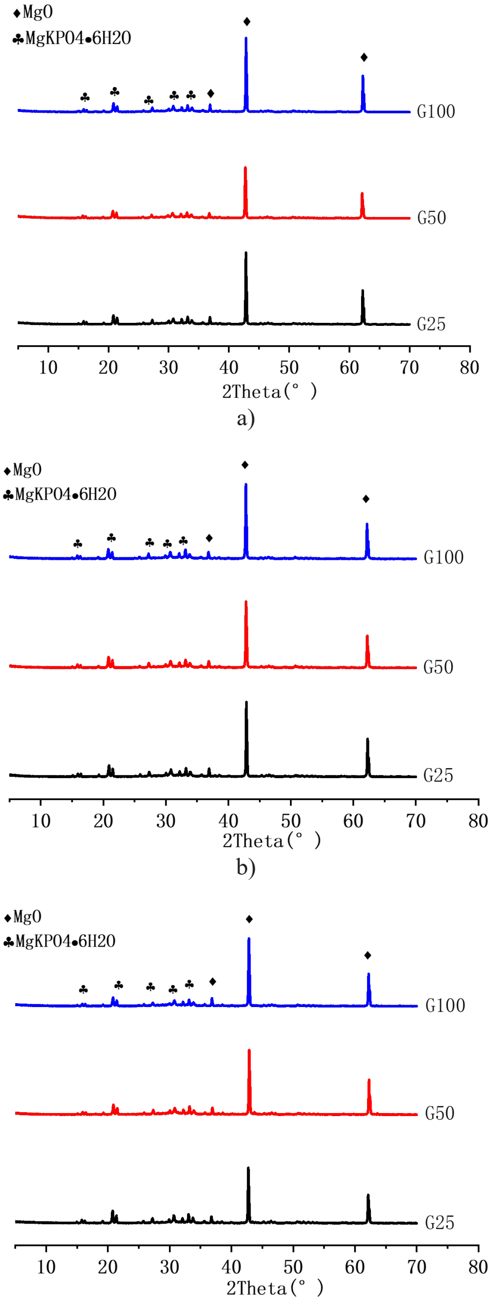

a)

b)

c)

Figure 7. XRD patterns of the MKPC: (a) T11, (b) T12, and (c) T13.

Table 5 lists the results obtained through the quantitative analysis using the software Jade 6.5. From Table 5, when the content of the impurity ions in the raw materials is the same, the increase in the calcination temperature is associated with an increase in the generation of the main hydration product MKP in the MKPC. Moreover, when the calcination temperature of the raw materials is the same, a decrease in the impurity ion content is associated with an increase in the production of MKP. This phenomenon indicates that increasing the calcination temperature and reducing the impurity ion content of the lithium-extracting magnesium slag can promote the formation of the main hydration product MKP in the MKPC.

Microscopic morphology of the MKPC

Figure 8a, b, c, d, e shows the SEM spectrum of each MKPC specimen after curing for 28 d. From Figure 8b, the hydration products of G50T12 were mainly tightly bound columnar or plate-like crystals. Some unreacted MgO particles are also included between the plate columnar crystals. Considering the size and structural composition, the plate columnar structure was determined to be K-struvite, the main hydration product of MKPC.

Under the same calcination condition of T12, the microscopic morphology of the G50T12 specimens had a large proportion of K-struvite as a whole; the structure was closely arranged, and the shape tended to be regular plate columnar. The plate columnar crystals were large, the surface was smooth, and more attachments appeared. The overall proportion of the K-struvite in the microscopic morphology of G25T12 and G100T12 was less than that of G50T12; the structure of the K-struvite was disordered and loose, and the size of plate-columnar crystals was small. In the microscopic morphology of G25T12, there were more agglomerated particles between the K-struvite than in G50T12, and the surface of the G100T12 crystals was covered or embedded with numerous unreacted MgO particles. The degree of the overlapping and interlacing of the crystal structures of G25T12 and G100T12 was greatly reduced by the influence of the MgO particles, and the overall structure was relatively loose. In addition, the internal microstructure of G50T11 indicates that some K-struvite was not completely reacted, with obvious defects in the overlapping of the crystal structures in the microstructure of G50T13. Therefore, G50T12 is the optimal process for preparing the MKPC in terms of the microstructure of the hydration products.

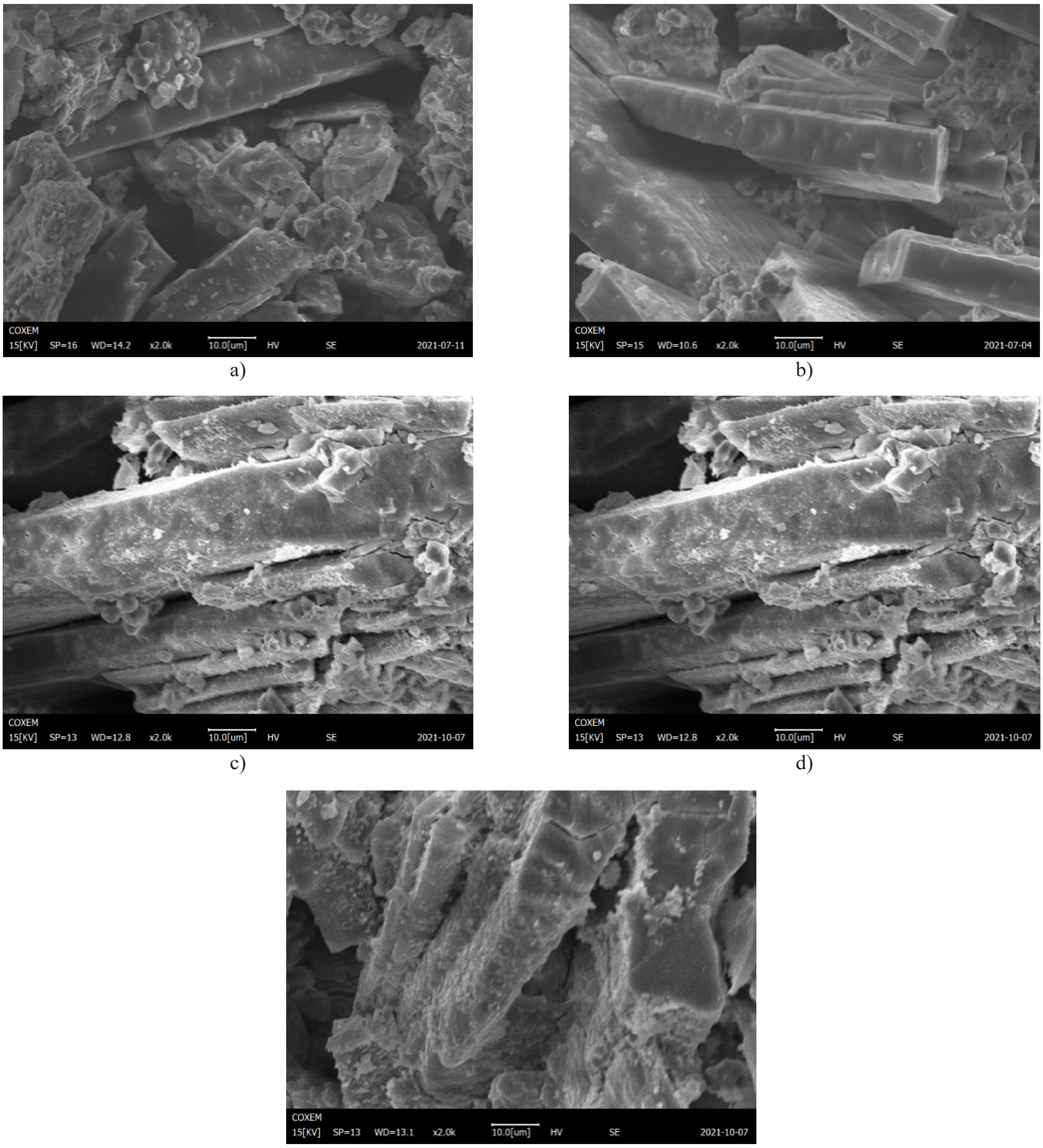

a) b) c) d) e)

Figure 8. SEM spectrum of the MKPC specimens: (a) G25T12, (b) G50T12, (c) G100T12, (d) G50T11, (e) G50T13.

Pore structure of the MKPC

Cement hydration products are closely related to the internal pore structure of cement slurries. The mechanical properties of cement are not only determined by the type and content of the hydration products but are also limited by the internal pores of the cement slurry. The porosity significantly affects the cement properties, such as the compressive strength, water absorption, and thermal conductivity. Figure 9 show the results of the mercury intrusion porosimetry analysis. Table 6 lists the statistical results of the pore size distribution of the MKPC samples after curing for 28 d. From Table 6, both the impurity ion content and calcination temperature of the lithium-extracting magnesium slag will affect the porosity of the MKPC. For example, the porosity of the G50T12 specimen is 27.8 %, whereas the porosity of the G25T12 and G100T12 specimens is 39.7 % and 40.3 %, respectively, which is 11.9 % and 12.5 % higher, respectively, than that of G50T12. Moreover, the porosity of the G50T11 and G50T13 specimens is 34.7 % and 41.5 %, respectively, which is an increase of 6.9 % and 13.7 %, respectively, compared to G50T12. This phenomenon shows that the porosity of the MKPC prepared using G50 is lower than that prepared using

Table 6. Statistical results of the pore size distribution of the MKPC samples after curing for 28 d.

Sample	Porosity (%)
G25T12	39.7
G50T12	27.8
G100T12	40.3
G50T11	34.7
G50T13	41.5

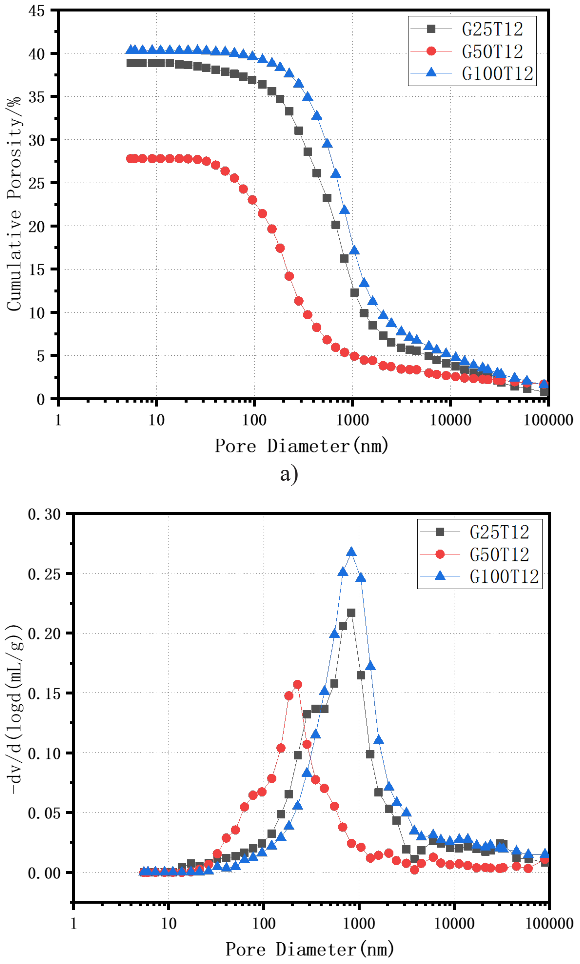

a)

b)

Figure 9. Cumulative porosity (a) and differential pore size distribution (b) of the MKPC cured for 28 d.

other impurity contents. The porosity of the MKPC prepared at T12 is lower than that of other calcination temperatures, and G50T12 is the process combination resulting in the lowest porosity.

CONCLUSIONS

In this study, the lithium-extracting magnesium slag extracted from a salt lake using the membrane separation method was used as a raw material to explore the influence of the impurity ion content in the lithium-extracting magnesium slag and the calcination temperature on the macroscopic properties and microstructure of the MKPC. The conclusions are as follows.

(1) For the same calcination temperature, washing to reduce the content of impurities, such as Cl^-, in the lithium-extracting magnesium slag is beneficial to improve the setting time and later strength of the MKPC. In G25, the washing was extensive, the content of the impurity ions is very low, and the hydration reaction of the MKPC was intense, resulting in a large temperature stress that is not conducive to the development of later strength. G50 can slow the hydration of the MKPC to the greatest extent without destroying the later strength and is the optimal impurity ion content.

(2) For the same impurity ion content, an increase in the calcination temperature results in an increased degree of crystallisation of the MgO, increased particle size, and decreased specific surface area. The compressive strength of the MKPC at a curing age of 28 days increased with an increase in the temperature. Increasing the calcination temperature is beneficial to prolong the setting time of the MKPC, and the difference in the specific surface area and activity of the MgO fired at T12 and T13 was small, with the same setting time. Combined with the economic and energy-saving benefits, T12 (1200 °C) is the most suitable temperature for the calcination of the lithium-extracting magnesium slag.

(3) Reducing the impurity ion content and increasing the calcination temperature can promote the formation of the main hydration product $MgKPO_4 \cdot 6H_2O$ in the MKPC. In the microscopic morphology of the G50T12 specimen, the K-struvite structure had the largest size, most regular arrangement, and lowest porosity. Combined with the comprehensive evaluation of the MKPC setting time, cube compressive strength development, porosity, and raw material production, G50T12 is determined to be the optimal treatment process for the preparation of MKPC.

Acknowledgments

This research was funded by the National Natural Science Foundations of China, grant number 52002202; Natural Science Foundation of Qinghai Province, grant number 2023-ZJ-914M.

REFERENCES

1. Xu B., Lothenbach B., Leemann A., Winnefeld F. (2018): Reaction mechanism of magnesium potassium phosphate cement with high magnesium-to-phosphate ratio. *Cement and Concrete Research, 108*, 140–151. doi:10.1016/j.cemconres.2018.03.013
2. Soudée E., Péra J. (2000): Mechanism of setting reaction in magnesia-phosphate cements. *Cement and Concrete Research, 30*(2), 315–321. doi:10.1016/s0008-

8846(99)00254-9

3. Yi G., Ma C., Long G., Zhao B., Xie Y. (2018): Effects of metakaolin on a novel aerated magnesium phosphate cement with high early strength. *Construction and Building Materials, 187*, 1130–1133. doi:10.1016/j.conbuildmat.2018.08.037
4. Qin J.H., Qian J.S., You C., et al. (2018): Bond behavior and interfacial micro-characteristics of magnesium phosphate cement onto old concrete substrate. *Construction and Building Materials, 167*, 166–176. doi:10.1016/j.conbuildmat.2018.02.018
5. Li Y., Bai W., Shi T. (2017): A study of the bonding performance of magnesium phosphate cement on mortar and concrete. *Construction and Building Materials, 142,* 459–468. doi:10.1016/j.conbuildmat.2017.03.090
6. Yang Q., Zhu B., Wu X. (2000): Characteristics and durability test of magnesium phosphate cement-based material for rapid repair of concrete, *Materials and Structures, 33*(4), 229–234, doi:10.1007/bf02479332
7. Jin B., Chen. L., Chen B. (2020): Factors assessment of a repair material for brick masonry loaded cracks using magnesium phosphate cement. *Construction and Building Materials, 252*, 119098. doi:10.1016/j.conbuildmat.2020.119098
8. Yang H.L., Fu M., Wu B.B., et al. (2019): Effect of Fe2O3 on the Immobilization of High-Level Waste with Magnesium Potassium Phosphate Ceramic. *Science and Technology of Nuclear Installations, 2019*, 1–10. doi:10.1155/2019/4936379
9. Mestres G., Ginebra M.P. (2011): Novel magnesium phosphate cements with high early strength and antibacterial properties. *Acta Biomaterialia 7*(4), 1853–1861. doi:10.1016/j.actbio.2010.12.008Z
10. Wu Z., Li F. (2001): Development of magnesium chloride resources in qinghai salt lake. *Salt Lake Research, 9*(2), 61–65.
11. Lahalle H., Coumes C.D.C., Mercier C., et al. (2018): Influence of the w/c ratio on the hydration process of a magnesium phosphate cement and on its retardation by boric acid. *Cement and Concrete Research, 109*, 159–174. doi:10.1016/j.cemconres.2018.04.010
12. Nie Z., Wu Q., Ding T., Bu L., Wang Y., Yu J. (2022): Hou Xianhua. Research progress of industrialization technology of lithium extraction from brine from salt lakes in China. *Inorganic Salt Industry, 54*(10), 1-12. doi: 10.19964/j.issn.1006-4990.2022-0542
13. Kentish S. E., Stevens G. W. (2001): Innovations in separations technology for the recycling and reuse of liquid waste streams. *Chemical Engineering Journal, 84*(2), 149–159. doi:10.1016/s1385-8947(01)00199-1
14. Xu N., Shi D., Li S., et al. (2017): Advances in extracting lithium from salt-lake brines by adsorption technique. *Materials Review, 31*(17), 116-121. doi: 10.11896/j.issn.1005-023X.2017.017.017
15. Li Z., Liu G., Tang F. (2017): Overview of Qinghai Salt Lake Lithium Resources and Lithium Extraction Technology. *Resource Information and Engineering, 32*(05): 94-97. doi: 10.19534/j.cnki.zyxxygc.2017.05. 045
16. Shi Y., Zhu C., Fan J., et al. (2018): Development status of lithium resources in Qinghai Salt Lake and suggestions for the development of lithium extraction industry. *Salt Lake Research, 2019*, 124-130. doi:10.12119/j.yhyj.201804002
17. Sivasankari J., Selvakumar S., Sivaji K., et al. (2014): Structural and optical characterization of MgO:X (X=Li, Na, and K) by solution combustion technique. *Journal of Alloy Compound, 2014*(616), 51–7. doi: 10.1016/j.jallcom.2014.07.052.
18. Li X., Bai L., Zhao H., Xiu Z., Huo D., Sun X. (2009): Study on the Influence of Chloride Ion on the Synthesis and Sintering Properties of Magnesium Oxide *Nano-powder. Functional Materials, 40*(07), 1215-1218.
19. Lee M.K., Kang S. (2018): A study of salt-assisted solution combustion synthesis of magnesium aluminate and sintering behaviour. *Ceramic International, 45*(6), 6665–72.Doi:10.1016/j.ceramint.2018.12.155
20. Eubank W.R. (1951): Calcination studies of magnesium oxides. *Journal of the American Ceramic Society, 34*(8), 225-229. doi:10.1111/j.1151-2916.1951.tb11644.x
21. Yang Q., Wu X. (1995): Research on new ultrafast hard phosphate repair materials. *Concrete and Cement Products, 6,* 13-15.
22. Yang J., Qian C., Zhang Q., Jiao B., Yan X. 2010): Effect of raw material particle size on hydration and hardening properties of magnesium phosphate cement. *Journal of Southeast University (Natural Science Edition), 40*(02), 373-379. doi:10.3969/j.issn.1001-0505.2010.02.03